Journal of *Marine Science and Engineering*

Article

Swarm Control for Connectivity-Preserving and Collision-Avoiding Unmanned Surface Vehicles Subject to Multiple Constraints

Guoqing Xia, Xianxin Sun * and Xiaoming Xia

College of Intelligent Systems Science and Engineering, Harbin Engineering University, Harbin 150001, China; xiaguoqing@hrbeu.edu.cn (G.X.); xia_xm@126.com (X.X.)

* Correspondence: hrbsunxianxin@hrbeu.edu.cn

Abstract: This paper investigates swarm control for unmanned surface vessels subject to multiple constraints. These constraints can be summarized as model parameter uncertainty, the unavailability of velocity measurements, time-varying environmental disturbances, input saturation and output constraints. Firstly, to recover unmeasured velocity information, to identify unknown vehicle dynamics and to estimate time-varying environmental disturbances, a neural adaptive state observer is designed for each vessel. Secondly, to avoid complex calculations, a second-order linear tracking differentiator is employed to generate a smooth reference signal and to extract the time derivative of the kinematic control law. Thirdly, to solve the input saturation, an auxiliary dynamic system is introduced. Fourthly, the barrier Lyapunov function is used to achieve connectivity preservation, collision avoidance and swarm control. Meanwhile, by using the estimated velocities of vessels, an output feedback controller is designed. The stability of the closed-loop system is proved. The simulation results show the effectiveness of the proposed swarm control strategy.

Keywords: swarm control; unmanned surface vehicles; multiple constraints; neural adaptive state observer; output feedback controller

Citation: Xia, G.; Sun, X.; Xia, X. Swarm Control for Connectivity-Preserving and Collision-Avoiding Unmanned Surface Vehicles Subject to Multiple Constraints. *J. Mar. Sci. Eng.* **2021**, *10*, 827. https://doi.org/10.3390/jmse10060827

Academic Editor: Alessandro Ridolfi

Received: 4 May 2022
Accepted: 15 June 2022
Published: 17 June 2022

1. Introduction

In recent years, the swarm control of multiple unmanned surface vehicles (USVs) has attracted extensive attention. The purpose of swarm control is to drive multiple agents to accomplish tasks uniformly, which is very different from the traditional control based on a single object [1]. Swarm control can be applied to a variety of tasks, such as arranging a group of USVs to form a safe area to protect other vessels [2,3], tracking floating pollutants [4], monitoring environment [5,6], etc. However, USVs will be affected by multiple constraints in operation. These constraints can be summarized as model parameter uncertainty, unavailability of velocity measurements, time-varying environmental disturbances, input saturation, and output constraints. These problems will reduce the performance of the system, and even lead to instability. Therefore, it is necessary to analyze these constraints and to design a swarm control strategy.

In applications, in addition to position information, velocity information is also very important. Generally, position information can be easily obtained by GNSS equipment, while velocity information may not be accurately computed by the GNSS receiver. In the high-speed operation of USVs, it is more difficult to obtain velocity information that is sufficiently timely for use in a control algorithm. Meanwhile, velocity obtained from position measurements by numerical differentiation techniques are often unfeasible due to inevitable measurement noises [7]. Therefore, it is significant to study output feedback schemes independent of the velocity measurement [8].

Some control strategies without velocity information have been proposed in the literature [9–13] such as the back-stepping observer approach [9], high-gain observer [10–12], passive nonlinear observer [13], etc. These control schemes have a common premise, that is, it is assumed that the vessel model parameter is known. However, due to imprecise measurements and external disturbances, accurate model parameters often cannot be obtained. In general, the hydrodynamic parameters of USVs are also time varying. It is emphasized that external disturbances and uncertainties can make the entire system unstable [14]. This increases the difficulty of measurement. In order to deal with uncertain dynamics, neural network (NN) approaches have been considered due to their inherent advantages including excellent approximation and learning performance [1,7,15–22].

Due to the power and response speed constraints of the vehicle's actuator, and the output constraints of the propeller, the vessel's control forces and moment cannot be infinite. Therefore, the amplitude of the control signal is usually limited to a certain range. Moreover, due to the requirements of different operational scenarios (e.g., acceleration from stationary to maximum speed, high sea state operation, etc.), the ship will have input saturation constraints. Otherwise, control input overshoot may occur, which will affect the performance of the control system and even lead to system instability. In [23], an adaptive steering control for uncertain ship dynamics with input constraints was designed. In [24], a dynamic surface control scheme was proposed for a class of uncertain strict-feedback nonlinear systems subject to input saturation. Furthermore, auxiliary dynamic systems have been used extensively for nonlinear systems design due to their efficiency and design flexibility [16,25–27].

In addition to input constraints, another challenge to swarm control for USVs is output (position) constraints. Prevailing collision avoidance approaches can be divided into two methodologies, potential functions [28–32] and prescribed performance functions [27,33–36]. Potential function approaches introduce a potential energy function that increases with the decrease in the distance between USVs. Then, a control low based on the gradient potential energy function is designed to minimize the potential energy of the system [28–32]. However, this method requires the design of another potential energy function in the Lyapunov function. Thus, there may be a conflict when choosing parameters that must simultaneously ensure the stability criteria are met and provide the required collision avoidance behavior. For the second method, the barrier Lyapunov function (BLF) is an effective way to prevent the violation of constraints for many practical systems. Many successful applications of this approach exist in the literature [27,33–36].

Motivated by the aforementioned observations, this work investigates the swarm control of USVs considering model uncertainties, the unavailability of velocity measurements, time-varying environmental disturbances, input saturation and output constraints. In summary, the main contributions are as follows.

1. A neural adaptive state observer is designed to recover velocity information and to estimate composite disturbances including model uncertainty and time-varying environmental disturbances.
2. An auxiliary dynamic system is introduced to deal with input saturation. A modified BLF is provided to achieve connectivity preservation, collision avoidance and swarm control.
3. In combination with the observer, an output feedback controller is proposed for the follower USVs based on a second-order linear tracking differentiator, an adaptive law, a modified BLF and graph theory. Meanwhile, the stability of the closed-loop system is proved via Lyapunov theory.

This paper is organized as follows. A table of notations and some variables used in the paper is presented (Table 1). Section 2 describes some preliminaries and mathematical modeling. Section 3 provides the neural adaptive state observer design. Section 4 presents the output feedback controller design and analyzes the stability by the Lyapunov method. Section 5 compares the results of simulations to verify the effectiveness of the proposed scheme. Section 6 concludes this paper.

Table 1. Notations and variables used in this paper.

Variable	Definition
$A \setminus B$	Set of elements belonging to A but not belonging to B
$\lvert\cdot\rvert$	Absolute value of a scalar
$\lVert\cdot\rVert$	Euclidean norm
$\mathbf{R}^{m\times n}$	$m \times n$ dimensional Euclidean space
$(\cdot)^{\mathrm{T}}$	Transpose of a matrix
$(\cdot)^{-1}$	Inverse of a matrix
$\otimes$	Kronecker product of matrix
$\mathcal{A} \in \mathbf{R}^{n\times n}$	Adjacency matrix defined as $\mathcal{A} = [a_{ij}]_{n\times n}$ with $a_{ij} = a_{ji}$
d_i	Defined as $d_i = \sum_{j=1}^{n} a_{ij}$
$\mathcal{D} \in \mathbf{R}^{n\times n}$	Degree matrix defined as $\mathcal{D}$ =diag$\{d_1, d_2, \ldots, d_n\}$
diag$\{d_i\}$	A block-diagonal matrix with d_i being the ith diagonal element
$\mathcal{L} \in \mathbf{R}^{n\times n}$	Laplacian matrix defined as $\mathcal{L} = \mathcal{D} - \mathcal{A}$
$\mathcal{B} \in \mathbf{R}^{n\times n}$	Information exchange matrix defined as $\mathcal{B} = \mathcal{L} - \mathcal{A}_0$
$\lambda_{\min}(\cdot)$	Minimum of eigenvalues of a matrix
$\lambda_{\max}(\cdot)$	Maximum of eigenvalues of a matrix
I_n	$n \times n$ dimensional identity matrix
0_n	$n \times n$ dimensional zero matrix

2. Preliminaries and Mathematical Modeling

2.1. Algebraic Graph Theory

Graph theory is used to describe the communication topology of n follower USVs and a virtual leader vehicle (denoted by 0). A directed graph $\mathcal{G} = (\mathcal{V}, \mathcal{E})$ consists of a vertex set $\mathcal{V} = \{0, 1, 2, \ldots, n\}$ and the set of edges $\mathcal{E} \subseteq \{(i, j) \in \mathcal{V} \times \mathcal{V}\}$. If $(i, j) \in \mathcal{E}$, node j is an adjacent node of node i. $\mathcal{N}_i = \{j \in \mathcal{V}, (i, j) \in \mathcal{E}\}$ represents the set of all adjacent nodes of node i, as can be seen in [37].

Consider a directed graph $\mathcal{G}$ composed of n nodes; the adjacency matrix $\mathcal{A} = [a_{ij}]_{n\times n}$ represents the link relationship between nodes, where $a_{ij} = 1$, if $(i, j) \in \mathcal{E}$; $a_{ij} = 0$, otherwise. If $a_{ij} = a_{ji}$, the graph is undirected; otherwise, it is directed. The Laplacian matrix is defined as $\mathcal{L} = \mathcal{D} - \mathcal{A}$, where $\mathcal{D}$= diag$\{d_1, d_2, \ldots, d_n\}$ with $d_i = \sum_{j=1}^{n} a_{ij}$.

In particular, a diagonal matrix $\mathcal{A}_0$ =diag$\{a_{i0}\}$ is defined as a leader adjacency matrix, where $a_{i0} = 1$, if and only if the ith USV receives information from the virtual leader vehicle; $a_{i0} = 0$, otherwise. Finally, the information exchange matrix is defined as $\mathcal{B} = \mathcal{L} + \mathcal{A}_0$.

Assumption 1. *The graph $\mathcal{G}$ is directed, and there is at least one spanning tree from root node to the leader node, i.e., $\mathcal{B}$ is a positive definite matrix.*

2.2. Barrier Lyapunov Function

Consider a continuous system

$$\dot{x} = f(x), x \in D, \tag{1}$$

where D is an open region containing the origin. If a continuously differentiable, positive definite function $V(x)$ satisfies $\lim_{x\to\partial D^-} V = +\infty$, and $V(x(t)) \leq b$, $\forall t \geq 0$, where $x(0) \in D$, $b > 0$ is a constant. Then, $V(x)$ is a barrier Lyapunov function, see [33,38].

A barrier Lyapunov function candidate is as follows

$$V = \frac{1}{2} \ln \frac{k^2}{k^2 - z^2}, \tag{2}$$

where $k > 0$ is a constant, $-k < z < k$.

The following lemma formalizes a result on the use of a BLF candidate for constraint satisfaction.

Lemma 1. *For any positive constant k, and any $z \in \mathbf{R}$ satisfying $-k < z < k$, we have*

$$\ln \frac{k^2}{k^2 - z^2} < \frac{z^2}{k^2 - z^2}. \tag{3}$$

Proof. Let $p1 = \frac{z^2}{k^2 - z^2} - \ln \frac{k^2}{k^2 - z^2}$, we have

$$p1 = \frac{z^2}{k^2 - z^2} - \ln(1 - \frac{z^2}{k^2 - z^2}). \tag{4}$$

As $-k < z < k$, one has $z^2 < k^2$. Then, we have the inequalities as follows:

$$0 \leq \frac{z^2}{k^2 - z^2} < \frac{k^2}{k^2 - z^2} = 1 - \frac{z^2}{k^2 - z^2}, \tag{5}$$

$$0 \leq \frac{z^2}{k^2 - z^2} < \frac{1}{2}, \tag{6}$$

Let $p2 = \frac{z^2}{k^2 - z^2}$, $p3 = -\ln(1 - p2) + p2$. The derivative of $p3$ is

$$\dot{p3} = \frac{2 - p2}{1 - p2} > 0. \tag{7}$$

This shows that $p3$ is continuously increasing and the minimum of $p3$ is $p3_{min} = 0$. Thus, we have $\ln \frac{k^2}{k^2 - z^2} < \frac{z^2}{k^2 - z^2}$. $\square$

2.3. Neural Network

For any real continuous function $f(\varsigma) : \mathbf{R}^n \to \mathbf{R}^k$ on a sufficiently large compact set Ω, there exists a radial basis function neural network (NN) such that

$$f(\varsigma) = W^{\mathrm{T}} h(\varsigma) + \varepsilon, \tag{8}$$

where input vector $\varsigma \in \Omega \subset \mathbf{R}^n$. $W = [\omega_1, \omega_2, \ldots, \omega_l]^{\mathrm{T}} \in \mathbf{R}^{k \times l}$ represents the output weight vector, satisfying $\|W\| \leq W^*$ with $W^* > 0$ being a positive constant. The NN node number $l > 1$. $h(\varsigma) = [h_1(\varsigma), \ldots, h_l(\varsigma)]^{\mathrm{T}}$. Since the neural function is bounded, there exists a positive constant $h_{\max} > 0$ such that $\|h(\varsigma)\| \leq h_{\max}$. $\varepsilon \in \mathbf{R}^k$ is the approximation error, satisfying $\|\varepsilon\| \leq \varepsilon^*$ with $\varepsilon^* > 0$ being a positive constant, see [22].

Define $\hat{W}$ as an estimate of W, and let the estimation error be denoted by $\tilde{W} = \hat{W} - W$. The optimal weight vector W is rewritten as

$$W = \arg \min_{\hat{W} \in \mathbf{R}^{m \times n}} \left\{ \sup_{\varsigma \in \Omega} \left| f(\varsigma) - \hat{W}^{\mathrm{T}} h(\varsigma) \right| \right\}, \tag{9}$$

In this paper, we choose $h_i(\varsigma)$ as a Gaussian function, as follows

$$h_i(\varsigma) = \exp\left\{ -\frac{(\varsigma - c_i)^{\mathrm{T}} (\varsigma - c_i)}{d_i^2} \right\}, \tag{10}$$

where $c_i = [c_{i1}, c_{i2}, \ldots, c_{in}]^{\mathrm{T}}$ is the center of the receptive field, and d_i is the width of the Gaussian function.

2.4. USVs Modeling

Consider a group of USVs consisting of a virtual leader vehicle (subscript 0) and n follower USVs (subscripts $1, 2, \ldots, n$). The 3-degree-of-freedom (DOFs) kinematics and dynamics equations of the ith USV can be expressed in vector form as [39]

$$\dot{\eta}_i = R_i(\psi_i)v_i, \tag{11}$$

$$M_i\dot{v}_i + D_iv_i = \tau_i + d_i, \tag{12}$$

where $R_i(\psi_i)$ is the rotation matrix, given as

$$R_i(\psi_i) = \begin{bmatrix} \cos(\psi_i) & -\sin(\psi_i) & 0 \\ \sin(\psi_i) & \cos(\psi_i) & 0 \\ 0 & 0 & 1 \end{bmatrix}, \tag{13}$$

with properties: $|R_i(\psi_i)| = 1$ and $R_i^{\mathrm{T}}(\psi_i)R_i(\psi_i) = I_3$. $\eta_i := [x_i, y_i, \psi_i]^{\mathrm{T}}$ is the position and yaw angle in the earth-fixed frame $X_EO_EY_E$ (see Figure 1). $v_i := [u_i, v_i, r_i]^{\mathrm{T}}$ is the velocity vector in the body-fixed frame $X_BO_BY_B$. The system inertia matrix $M_i \in \mathbf{R}^{3\times3}$ is positive definite and constant. The damping matrix $D_i \in \mathbf{R}^{3\times3}$ is also defined as symmetric and positive. The control input $\tau_i := [\tau_{i1}, \tau_{i2}, \tau_{i3}]^{\mathrm{T}}$ is the control input, which is produced by the a propeller and a rudder, etc. $d_i := [d_{i1}, d_{i2}, d_{i3}]^{\mathrm{T}}$ is a time-varying environmental disturbance.

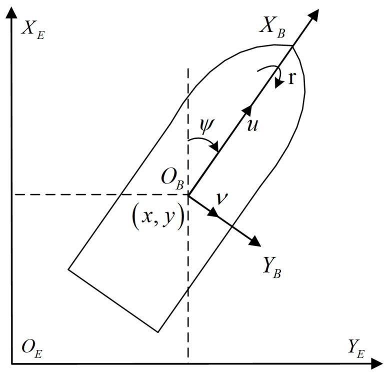

Figure 1. Earth-fixed frame and body-fixed frame.

In this paper, the input saturation can be described as

$$\tau_i = \begin{cases} \tau_{i,\max}, & \text{if } \tau_{ic} > \tau_{i,\max} \\ \tau_{ic}, & \text{if } \tau_{i,\min} \le \tau_{ic} \le \tau_{i,\max} \\ \tau_{i,\min}, & \text{if } \tau_{ic} < \tau_{i,\min} \end{cases}, \tag{14}$$

where $\tau_{i,\max} \in \mathbf{R}^3$ and $\tau_{i,\min} \in \mathbf{R}^3$ are the maximum and minimum control forces and moment of the ith vehicle, respectively. $\tau_{ic} = [\tau_{ic1}, \tau_{ic2}, \tau_{ic3}]^{\mathrm{T}}$ is calculated by the controller.

The main goal of this paper is to design an output feedback controller for each USV to track the reference signal (η_d) subject to model uncertainties and input constraints only using position measurements. Specifically, it is to achieve the following objectives.

(1) Formation objective: the ith USV is driven to a formation pattern with relative position and heading, and we have:

$$\lim_{t\to+\infty} \|\eta_i - \eta_d - \mu_i\| \le \sigma_i, \tag{15}$$

where $\eta_i := [x_i, y_i, \psi_i]^{\mathrm{T}}$. $\eta_d := [x_d, y_d, \psi_d]^{\mathrm{T}}$ is the desired reference point. $\mu_i := [x_{i\mu}, y_{i\mu}, \psi_{i\mu}]^{\mathrm{T}}$ represents the expected offset of the vehicle's position and heading relative to the desired reference point, which is the position of the virtual leader. To maintain the USVs in a fixed formation, μ_i is a constant vector. $\sigma_i > 0$ is a constant.

(2) Collision avoidance: the position for ith USV must remain within the set

$$\Omega_{\eta_i} = \{|\eta_i - \mu_i| < k_{ic}\}, \tag{16}$$

where $k_{ic} = \frac{k_{ib}}{\lambda_{\min}(\mathcal{H})} + \eta_d + \mu_i$, see Section 4.3 for details.

Assumption 2. *The reference signal η_d is smooth and differentiable everywhere. Its first derivative $\dot{\eta}_d$ and second derivative $\ddot{\eta}_d$ exist and are bounded.*

Assumption 3. *The coincident disturbances, which mainly include model uncertainties and time-varying environmental disturbances, are bounded.*

Assumption 4. *The position of each USV is available.*

Assumption 5. *The initial positions of USVs are meeting the maximum collision avoidance distance, i.e., $z_{i1}(0) \in \Omega_{z_{i1}}, i = 1, \ldots, n$. USVs are always within the communication range.*

2.5. Environmental Disturbances Modeling

Unmodeled external forces and moments due to wind, ocean currents, and second waves are lumped together into an earth-fixed slowly varying bias term $d_i \in \mathbf{R}^3$ [13,40]. A widely used bias model for USVs is the first-order Markov process. In this paper, the environmental disturbances are modeled as

$$d_i = -R_i^{\mathrm{T}} b, \tag{17}$$

where b represents a first-order Markov process, given as

$$\dot{b} = -\mathrm{T}^{-1} b + \mathrm{E}_b \vartheta_b, \tag{18}$$

where $\mathrm{T} \in \mathbf{R}^{3\times3}$ is a diagonal matrix of positive bias time constants, $\mathrm{E}_b \in \mathbf{R}^{3\times3}$ is a diagonal matrix scaling the amplitude of ϑ_b, and $\vartheta_b \in \mathbf{R}^3$ is a vector of zero-mean Gaussian white noise.

Remark 1. *The USV in this paper has a low speed and the part above the waterline (i.e., super-structure) is small, and only calm sea conditions are considered in this paper. Therefore, the impact of sea wind on the USV is ignored. Because the draft of the USV is very shallow, the ocean current has little impact on it. Therefore, the impact of the ocean current on the USV is not considered. The wave disturbance consists of a low-frequency part and high-frequency part. The oscillation motion caused by the high-frequency part shall not enter the feedback control circuit. In this paper, only the low-frequency part is considered during the control process.*

3. Neural Adaptive State Observer Design

In engineering applications, the parameters M_i and D_i cannot always be measured accurately. Under such circumstances, according to Equations (11) and (12), an approximate model for the dynamics of the ith USV can be written as

$$\dot{\eta}_i = R_i v_i, \tag{19}$$

$$\overline{M}_i \dot{v}_i = \tau_i - f_i(v_i), \tag{20}$$

where $\overline{M}_i^{\mathrm{T}} = \overline{M}_i$ is the nominal inertial matrix, which is positive definite. A new variable ς_i is used as the input vector of the NN. $\varsigma_i = [\eta_i^{\mathrm{T}}, \eta_i^{\mathrm{T}}(t-t_d), \eta_i^{\mathrm{T}}(t-2\,t_d), \tau_i^{\mathrm{T}}]^{\mathrm{T}}$, and t_d is a positive constant. In Equation (8), the $f_i(v_i) = [f_{i1}, f_{i2}, f_{i3}]^{\mathrm{T}}$ is written as

$$f_i(v_i) = W_i^{\mathrm{T}} h_{ij}(\varsigma_i) + \varepsilon_i, \tag{21}$$

where $W_i = [W_{i1}, W_{i2}, W_{i3}]^{\mathrm{T}} \in \mathbf{R}^{m\times 3}$. $j = 1, 2, \ldots, m$ represents the jth neuron. $\varepsilon_i \in \mathbf{R}^3$ is the approximation error, satisfying $\|\varepsilon_i\| \le \varepsilon_{i,\max}$ with $\varepsilon_{i,\max} \in \mathbf{R}$ being a positive constant. $h_{ij}(\varsigma_i) \in \mathbf{R}^{m\times 1}$, which satisfies $\|h_{ij}(\varsigma_i)\| \le h_{ij,\max}$ with $h_{ij,\max} \in \mathbf{R}$ being a positive constant.

Let $\hat{\eta}_i = [\hat{x}_i, \hat{y}_i, \hat{\psi}_i]^{\mathrm{T}}$ represent an estimation of η_i, and $\hat{v}_i = [\hat{u}_i, \hat{v}_i, \hat{r}_i]^{\mathrm{T}}$ represent an estimate of v_i. Define the position estimation error as $\tilde{\eta}_i = \hat{\eta}_i - \eta_i$. We design a neural adaptive state observer (NASO) as

$$\dot{\hat{\eta}}_i = R_i \hat{v}_i - K_{oi1}\tilde{\eta}_i, \tag{22}$$

$$\overline{M}_i \dot{\hat{v}}_i = \tau_i - \hat{W}_i^{\mathrm{T}} h_{ij}(\varsigma_i) - K_{oi2} R_i^{\mathrm{T}} \tilde{\eta}_i, \tag{23}$$

where $K_{oi1} \in \mathbf{R}^{3\times 3}$ and $K_{oi2} \in \mathbf{R}^{3\times 3}$ are positive definite diagonal gain matrices. $\hat{W}_i = [\hat{W}_{i1}, \hat{W}_{i2}, \hat{W}_{i3}]^{\mathrm{T}}$ is an estimate of W_i. We design a weight adaptive update law for $\hat{W}_i$ as

$$\dot{\hat{W}}_{ik} = \gamma_{ik} h_{ij}(\varsigma_i) p_{ik} - k_{iw}\hat{W}_{ik}, k = 1, 2, 3 \tag{24}$$

where $p_{ik} = \tilde{\eta}_i^{\mathrm{T}} R_i = [p_{i1}, p_{i2}, p_{i3}]$, and $\gamma_{ik} > 0$ and $k_{iw} > 0$ are constants.

Define the velocity estimation error as $\tilde{v}_i = \hat{v}_i - v_i$. Based on the above analysis, the dynamic error estimation equations of the NASO can be written as

$$\dot{\tilde{\eta}}_i = R_i \tilde{v}_i - K_{oi1}\tilde{\eta}_i, \tag{25}$$

$$\overline{M}_i \dot{\tilde{v}}_i = -\tilde{W}_i^{\mathrm{T}} h_{ij}(\varsigma_i) - K_{oi2} R_i^{\mathrm{T}} \tilde{\eta}_i + \varepsilon_i, \tag{26}$$

To facilitate the stability analysis of the NASO, a new variable $X_i = [\tilde{\eta}_i^{\mathrm{T}}, \tilde{v}_i^{\mathrm{T}}]^{\mathrm{T}}$ is defined. Equations (25) and (26) then become

$$\dot{X}_i = A_i X_i + B_i\left(-\tilde{W}_i^{\mathrm{T}} h_{ij}(\varsigma_i) + \varepsilon_i\right), \tag{27}$$

$$\tilde{\eta}_i = C_i X_i, \tag{28}$$

where A_i, B_i and C_i are defined as:

$$A_i = \begin{bmatrix} -K_{oi1} & R_i \\ -K_{oi2}\overline{M}_i^{-1} R_i^{\mathrm{T}} & 0_3 \end{bmatrix}, B_i = \begin{bmatrix} 0_3 \\ \overline{M}_i^{-1} \end{bmatrix}, \quad C_i = \begin{bmatrix} I_3 & 0_3 \end{bmatrix}. \tag{29}$$

For convenience, a variable $\chi_i = T_i X_i$ is introduced with $T_i = \mathrm{diag}\{R_i^{\mathrm{T}}, I_3\}$. Then, (27) can be written as

$$\dot{\chi}_i = (A_{i0} + r_i S_T)\chi_i + B_i\left(-\tilde{W}_i^{\mathrm{T}} h_{ij}(\varsigma_i) + \varepsilon_i\right), \tag{30}$$

where r_i is the yaw rate, $S_T = \mathrm{diag}\{S^{\mathrm{T}}, 0_3\}$, and S and A_{i0} are defined as:

$$S = \begin{bmatrix} 0 & -1 & 0 \\ 1 & 0 & 0 \\ 0 & 0 & 0 \end{bmatrix}, A_{i0} = \begin{bmatrix} -K_{oi1} & I_3 \\ -K_{oi2}\overline{M}_i^{-1} & 0_3 \end{bmatrix}. \tag{31}$$

Similarly, Equation (24) is written as

$$\dot{\hat{W}}_{ik} = \gamma_{ik} h_{ij}(\varsigma_i) s_{ik} - k_{iw}\hat{W}_{ik}, k = 1, 2, 3 \tag{32}$$

where $s_{ik} = \chi_i^{\mathrm{T}} C_i^{\mathrm{T}} = [s_{i1}, s_{i2}, s_{i3}]$.

Using this notation, we can show that the following theorem holds:

Theorem 1. *The NASO estimation error is bounded; if the NASO is defined using Equations (27) and (28), the weight adaptive update law is defined using Equation (32), the parameters satisfy* $k_{iw} - \gamma_{ik} h_{ij,\max}^2 > 0$ *and there exist positive definite symmetric matrices* $Q_i, P_i \in \mathbf{R}^{6\times 6}$ *such that the linear matrix inequalities (LMIs) are satisfied:*

$$\begin{aligned} A_{i0}^{\mathrm{T}} P_i + P_i A_{i0} + P_i B_i B_i^{\mathrm{T}} P_i + Q_i \\ + F_i F_i^{\mathrm{T}} + r_{i,\max} (S_T^{\mathrm{T}} P_i + P_i S_T) \leq 0, \end{aligned} \tag{33}$$

$$\begin{aligned} A_{i0}^{\mathrm{T}} P_i + P_i A_{i0} + P_i B_i B_i^{\mathrm{T}} P_i + Q_i \\ + F_i F_i^{\mathrm{T}} - r_{i,\max} (S_T^{\mathrm{T}} P_i + P_i S_T) \leq 0, \end{aligned} \tag{34}$$

where $F_i = C_i^{\mathrm{T}} - P_i B_i$; $r_{i,\max}$ *is the upper bound of* r_i, *satisfying* $\|r_i\| \leq r_{i,\max}$ *with* $r_{i,\max} \in \mathbf{R}$ *being a positive constant.*

Proof. We choose the Lyapunov function V_{io} as

$$V_{io} = \frac{1}{2} \chi_i^{\mathrm{T}} P_i \chi_i + \frac{1}{2} \sum_{k=1}^{3} \frac{1}{\gamma_{ik}} \tilde{W}_{ik}^{\mathrm{T}} \tilde{W}_{ik}, \tag{35}$$

The time derivative of V_{io} is

$$\begin{aligned} \dot{V}_{io} =& \frac{1}{2} \chi_i^{\mathrm{T}} \Big(P_i A_{i0} + A_{i0}^{\mathrm{T}} P_i + r_i P_i S_T + r_i S_T^{\mathrm{T}} P_i \Big) \chi_i \\ &+ \chi_i^{\mathrm{T}} P_i B_i \Big(-\tilde{W}_i^{\mathrm{T}} h_{ij}(\varsigma_i) + \varepsilon_i \Big) + \sum_{k=1}^{3} \frac{1}{\gamma_{ik}} \tilde{W}_{ik}^{\mathrm{T}} \dot{\tilde{W}}_{ik} \end{aligned} \tag{36}$$

Let $\lambda_i = \frac{1}{2} \chi_i^{\mathrm{T}} (P_i A_{i0} + A_{i0}^{\mathrm{T}} P_i + r_i P_i S_T + r_i S_T^{\mathrm{T}} P_i) \chi_i + \chi_i^{\mathrm{T}} P_i B_i (-\tilde{W}_i^{\mathrm{T}} h_{ij}(\varsigma_i) + \varepsilon_i)$, then

$$\begin{aligned} \dot{V}_{io} =& \lambda_i + \sum_{k=1}^{3} \frac{1}{\gamma_{ik}} \tilde{W}_{ik}^{\mathrm{T}} \dot{\tilde{W}}_{ik} \\ =& \lambda_i + \sum_{k=1}^{3} \frac{1}{\gamma_{ik}} \tilde{W}_{ik}^{\mathrm{T}} (\dot{\hat{W}}_{ik} - \dot{W}_{ik}) \\ =& \lambda_i + \sum_{k=1}^{3} \tilde{W}_{ik}^{\mathrm{T}} h_{ij}(\varsigma_i) s_{ik} - \sum_{k=1}^{3} \frac{k_{iw}}{\gamma_{ik}} \tilde{W}_{ik}^{\mathrm{T}} \hat{W}_{ik} \\ =& \lambda_i + \tilde{W}_i^{\mathrm{T}} h_{ij}(\varsigma_i) \chi_i^{\mathrm{T}} C_i^{\mathrm{T}} - \sum_{k=1}^{3} \frac{k_{iw}}{\gamma_{ik}} \tilde{W}_{ik}^{\mathrm{T}} \hat{W}_{ik} \end{aligned} \tag{37}$$

Substituting Equations (33) and (34) into (37), then

$$\begin{aligned} \dot{V}_{io} \leq& \frac{1}{2} \chi_i^{\mathrm{T}} \Big(P_i A_{i0} + A_{i0}^{\mathrm{T}} P_i + r_i P_i S_T + r_i S_T^{\mathrm{T}} P_i \Big) \chi_i \\ &+ \chi_i^{\mathrm{T}} F_i \tilde{W}_i^{\mathrm{T}} h_{ij}(\varsigma_i) + \chi_i^{\mathrm{T}} P_i B_i \varepsilon_i - \sum_{k=1}^{3} \frac{k_{iw}}{\gamma_{ik}} \tilde{W}_{ik}^{\mathrm{T}} \hat{W}_{ik} \end{aligned} \tag{38}$$

Using Young's inequality [41], we have

$$
\begin{aligned}
\chi_i^{\mathrm{T}} F_i \tilde{W}_i^{\mathrm{T}} h_{ij}(\varsigma_i) &\le \frac{1}{2}\chi_i^{\mathrm{T}} F_i F_i^{\mathrm{T}} \chi_i + \frac{h_{ij,\max}^2}{2} \tilde{W}_i^{\mathrm{T}} \tilde{W}_i \\
\chi_i^{\mathrm{T}} P_i B_i \varepsilon_i &\le \frac{1}{2}\chi_i^{\mathrm{T}} P_i B_i B_i^{\mathrm{T}} P_i \chi_i + \frac{1}{2}\varepsilon_{i,\max}^2 \\
-\tilde{W}_{ik}^{\mathrm{T}} \hat{W}_{ik} &= -\tilde{W}_{ik}^{\mathrm{T}} (\tilde{W}_{ik} + W_{ik}) \\
&\le -\|\tilde{W}_{ik}\|^2 + \left(\frac{1}{2}\|\tilde{W}_{ik}\|^2 + \frac{1}{2}\|W_{ik}\|^2\right) \\
&\le -\frac{1}{2}\|\tilde{W}_{ik}\|^2 + \frac{1}{2}\|W_{ik}\|^2
\end{aligned} \tag{39}
$$

Substituting Equation (39) into (38), then

$$
\begin{aligned}
\dot{V}_{io} \le& \frac{1}{2}\chi_i^{\mathrm{T}}\left(P_i A_{i0} + A_{i0}^{\mathrm{T}} P_i + r_i P_i S_T + r_i S_T^{\mathrm{T}} P_i + F_i F_i^{\mathrm{T}} + P_i B_i B_i^{\mathrm{T}} P_i\right)\chi_i \\
&+ \frac{h_{ij,\max}^2}{2} \tilde{W}_i^{\mathrm{T}} \tilde{W}_i + \frac{1}{2}\varepsilon_{i,\max}^2 + \sum_{k=1}^{3} \frac{k_{iw}}{2\gamma_{ik}}\left(-\|\tilde{W}_{ik}\|^2 + \|W_{ik}\|^2\right)
\end{aligned} \tag{40}
$$

Substituting Equations (33) and (34) into (40), then

$$
\begin{aligned}
\dot{V}_{io} \le& -\frac{1}{2}\lambda_{\min}(Q_i)\|\chi_i\|^2 - \sum_{k=1}^{3} \frac{1}{2\gamma_{ik}}\left(k_{iw} - \gamma_{ik} h_{ij,\max}^2\right)\|\tilde{W}_{ik}\|^2 \\
&+ \sum_{k=1}^{3} \frac{k_{iw}}{2\gamma_{ik}}\|W_{ik}\|^2 + \frac{1}{2}\varepsilon_{i,\max}^2 \\
\le& -a_{i1} V_{io} + a_{i2}
\end{aligned} \tag{41}
$$

As a result of the above control low, $\dot{V}_{io} \le -a_{i1} V_{io} + a_{i2}$ and this results in the ultimately uniformly bounded regulation of the state.

Then, Equation (41) can be written as

$$
\dot{V}_{io}(t) \le -a_{i1} V_{io}(t) + a_{i2}, \tag{42}
$$

where $a_{i1} = \min\left\{\frac{\lambda_{\min}(Q_i)}{\lambda_{\max}(P_i)}, k_{iw} - \gamma_{ik} h_{ij,\max}^2\right\} > 0$, and $a_{i2} = \sum_{k=1}^{3} \frac{k_{iw}}{2\gamma_{ik}}\|W_{ik}\|^2 + \frac{1}{2}\varepsilon_{i,\max}^2$, $0 < a_{i2} \le a_{i2,\max}$ with $a_{i2,\max} \in \mathbf{R}$ being a positive constant.

The coefficients in the observer design process are determined by Equation (42). Since the observer design process needs to meet the Lyapunov theory, the selection of parameters needs to meet Equation (42).

Then, Equation (42) becomes

$$
V_{io}(t) \le \left[V_{io}(0) - \frac{a_{i2}}{a_{i1}}\right] e^{-a_{i1} t} + \frac{a_{i2}}{a_{i1}}, \tag{43}
$$

From Equation (43), when $t \to \infty$, $V_{io} \to \frac{a_{i2}}{a_{i1}}$. Thus, the signals in closed-loop are bounded. Then, the states χ_i are bounded. Noticing $T_i^{\mathrm{T}} = T_i^{-1}$, $\|T_i^{\mathrm{T}}\| \le 1$ and using $X_i = T_i^{\mathrm{T}} \chi_i$, the estimation error signal X_i is bounded.

This completes the proof. □

4. Output Feedback Controller Design

Firstly, a neural network adaptive state observer is designed, which can reconstruct the velocities and estimate the coincidence disturbances. Secondly, an ADS is designed to deal with the problem of input saturation. Thirdly, in order to solve the problem that the first-order filter is sensitive to noise in the traditional dynamic surface control technology, a second-order linear tracking differentiator (SOLTD) is introduced. Then, an output feedback controller is designed, as shown in Figure 2.

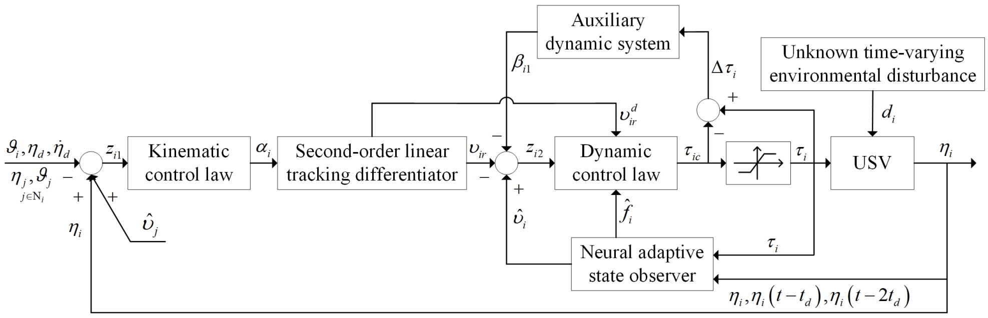

Figure 2. The structure diagram of swarm control for USVs.

4.1. Auxiliary Dynamic System

In this subsection, an auxiliary dynamic system (ADS) is introduced to solve the input saturation problem, as can be seen in Figure 2. For ADS, the system input is the deviation ($\Delta\tau_i$), the output is the velocity tracking error compensation (β_{i1}) for ith USV. The ADS is designed as

$$\dot{\beta}_{i1} = -L_{i1}\beta_{i1} + \overline{M}_i^{-1}\Delta\tau_i \tag{44}$$

where $L_{i1} \in \mathbf{R}^{3\times 3}$ is a positive definite diagonal matrix. $\Delta\tau_i = \tau_i - \tau_{ic}$, $\|\Delta\tau_i\| \leq \Delta\tau_{i,\max}$, $\Delta\tau_{i,\max} > 0$ is a constant.

4.2. Output Feedback Controller Design

In this subsection, an output feedback controller for multiple USVs is designed using dynamic surface control technology. The design process is divided into the following steps.

Step 1: According to the communication topology between USVs, the first tracking error of the ith USV in the earth-fixed frame is defined as

$$z_{i1} = \sum_{j\in\mathcal{N}_i} a_{ij}\left(\eta_i - \eta_j - \mu_{ij}\right) + a_{i0}(\eta_i - \eta_d - \mu_i), \tag{45}$$

where $\mathcal{N}_i$, a_{ij} and a_{i0} are defined in Section 2.1. η_i, η_d and μ_i are explained in Equation (15), η_j has similar definition, $\mu_{ij} = \mu_i - \mu_j$.

For the time derivative of z_{i1}, we obtain

$$\dot{z}_{i1} = a_{id}R_i v_i - \sum_{j\in\mathcal{N}_i} a_{ij}R_j v_j - a_{i0}\dot{\eta}_d, \tag{46}$$

where $a_{id} = d_i + a_{i0}$, d_i and a_{i0} are defined in Section 2.1.

The kinematic control low (α_i) of the ith USV is designed as

$$\alpha_i = \frac{R_i^{\mathrm{T}}}{a_{id}}\left\{-K_{i1}z_{i1} - \kappa_{ia}z_{i3} + \sum_{j\in\mathcal{N}_i} a_{ij}R_j\hat{v}_j + a_{i0}\dot{\eta}_d\right\} \tag{47}$$

where $K_{i1} \in \mathbf{R}^{3\times 3}$ is a positive definite diagonal matrix. $\kappa_{ia} = 2a_{id} + \frac{d_i}{2} > 0$ is a constant. $z_{i3} = [z_{i3,1}, z_{i3,2}, z_{i3,3}]^{\mathrm{T}}$ with $z_{i3,l} = \frac{z_{i1,l}}{k_{ib,l}^2 - z_{i1,l}^2}$, $l = 1,2,3$, $z_{i1} = [z_{i1,1}, z_{i1,2}, z_{i1,3}]^{\mathrm{T}}$. Define a compact set $\Omega_{z_{i1}} = \{z_{i1} \mid -k_{ib} < z_{i1} < k_{ib}\}$, where $k_{ib} = [k_{ib,1}, k_{ib,2}, k_{ib,3}]^{\mathrm{T}}$. Similarly, R_j is the rotation matrix of jth USV. $\hat{v}_j$ is the velocity vector estimation value.

To avoid the calculation of the time derivative of α_i, and considering the noise sensitivity of the first-order low-pass filter, a SOLTD is introduced as follows

$$\begin{cases} \dot{v}_{ir} = v_{ir}^d \\ \dot{v}_{ir}^d = -\iota_i^2(v_{ir} - \alpha_i) - 2\iota_i v_{ir}^d \end{cases} \tag{48}$$

where $\iota_i > 0$ is a time constant, $v_{ir} \in \mathbf{R}^3$ is the output vector of SOLTD.

Step 2: The second tracking error of the ith USV in earth-fixed frame is defined as

$$z_{i2} = \hat{v}_i - v_{ir} - \beta_{i1}. \tag{49}$$

Using the Equations (23) and (44), the time derivative of z_{i2}, we have

$$\overline{M}_i \dot{z}_{i2} = -K_{oi2} R_i^{\mathrm{T}} \tilde{\eta}_i - \hat{W}_i h_{ij}(\varsigma_i) + \tau_{ic} - \overline{M}_i(v_{ir}^d - L_{i1}\beta_{i1}) \tag{50}$$

The dynamic equation of the ith USV is designed as

$$\tau_{ic} = -K_{i2} z_{i2} + \hat{W}_i h_{ij}(\varsigma_i) + \overline{M}_i(v_{ir}^d - L_{i1}\beta_{i1}). \tag{51}$$

where $K_{i2} \in \mathbf{R}^{3\times 3}$ is a positive definite diagonal matrix.

Substituting Equations (47) and (51) into (46) and (50), we obtain

$$\begin{aligned} \dot{z}_{i1} = &- K_{i1} z_{i1} - k_{ia} z_{i3} + a_{id} R_i(-\tilde{v}_i + \beta_{i1} + \hat{z}_{i2} \\ &+ q_i) + d_i R_j \tilde{v}_j, \end{aligned} \tag{52}$$

$$\overline{M}_i \dot{z}_{i2} = -K_{i2} z_{i2} - K_{oi2} R_i^{\mathrm{T}} \tilde{\eta}_i, \tag{53}$$

where $q_i = v_{ir} - \alpha_i$, $\|q_i\| \leq q_{i,\max}$, $q_{i,\max} > 0$ is a constant.

4.3. Stability Analysis

Theorem 2. *Consider a closed-loop system subject to model parameter uncertainties, velocity measurements not being available, time-varying environmental disturbances, input saturation and output constraints. Let the USV dynamics be given by Equations (19) and (20), NASO by Equations (22) and (23), weight adaptive update law by Equation (24), ADS by (44), and kinematic and dynamic equations by Equations (47) and (51). Suppose that the closed-loop system satisfies Assumptions 1–5. Then, the following statements hold.*

(i) All signals in the closed-loop system are uniformly ultimately bounded.
(ii) All USVs track the reference signal with a bounded tracking error.
(iii) The output position of each USV satisfies output constraints.

Proof. Consider the above closed-loop system, and the Lyapunov function V_i is chosen as

$$V_i = \frac{1}{2}\sum_{i=1}^{n}\left\{2V_{io} + \sum_{l=1}^{3}\ln\frac{k_{ib,l}^2}{k_{ib,l}^2 - z_{i1,l}^2} + z_{i2}^{\mathrm{T}}\overline{M}_i z_{i2} + \beta_{i1}^{\mathrm{T}}\beta_{i1}\right\} \tag{54}$$

For the time derivative of V_i, we obtain

$$\begin{aligned} \dot{V}_i &= \sum_{i=1}^{n}\{\dot{V}_{io} + z_{i3}^{\mathrm{T}}\dot{z}_{i1} + z_{i2}^{\mathrm{T}}\overline{M}_i\dot{z}_{i2} + \beta_{i1}^{\mathrm{T}}\dot{\beta}_{i1}\} \\ &= \sum_{i=1}^{n}\{\dot{V}_{io} - z_{i3}^{\mathrm{T}}K_{i1}z_{i1} - k_{ia}z_{i3}^{\mathrm{T}}z_{i3} + z_{i3}^{\mathrm{T}}[a_{id}R_i(-\tilde{v}_i \\ &\qquad + \beta_{i1} + \hat{z}_{i2} + q_i) + d_iR_j\tilde{v}_j] - z_{i2}^{\mathrm{T}}K_{i2}z_{i2} \\ &\qquad - z_{i2}^{\mathrm{T}}K_{oi2}R_i^{\mathrm{T}}\tilde{\eta}_i - \beta_{i1}^{\mathrm{T}}L_{i1}\beta_{i1} + \beta_{i1}^{\mathrm{T}}\overline{M}_i^{-1}\Delta\tau_i\} \end{aligned} \tag{55}$$

Using Young's inequality [41], we have

$$\begin{aligned}
-z_{i3}^{\mathrm{T}} a_{id} R_i \tilde{v}_i &\leq \frac{a_{id}}{2} z_{i3}^{\mathrm{T}} z_{i3} + \frac{a_{id}}{2} \|\tilde{v}_i\|^2 \\
z_{i3}^{\mathrm{T}} a_{id} R_i \beta_{i1} &\leq \frac{a_{id}}{2} z_{i3}^{\mathrm{T}} z_{i3} + \frac{a_{id}}{2} \|\beta_{i1}\|^2 \\
z_{i3}^{\mathrm{T}} a_{id} R_i z_{i2} &\leq \frac{a_{id}}{2} z_{i3}^{\mathrm{T}} z_{i3} + \frac{a_{id}}{2} \|z_{i2}\|^2 \\
z_{i3}^{\mathrm{T}} a_{id} R_i q_i &\leq \frac{a_{id}}{2} z_{i3}^{\mathrm{T}} z_{i3} + \frac{a_{id}}{2} q_{i,\max}^2 \\
z_{i3}^{\mathrm{T}} d_i R_j \tilde{v}_j &\leq \frac{d_i}{2} z_{i3}^{\mathrm{T}} z_{i3} + \frac{d_i}{2} \|\tilde{v}_j\|^2 \\
-z_{i2}^{\mathrm{T}} K_{oi2} R_i^{\mathrm{T}} \tilde{\eta}_i &\leq \frac{\lambda_{\max}(K_{oi2})}{2} \left(\|z_{i2}\|^2 + \|\tilde{\eta}_i\|^2 \right) \\
\beta_{i1}^{\mathrm{T}} \overline{M}_i^{-1} \Delta\tau_i &\leq \frac{\lambda_{\max}(\overline{M}_i^{-1})}{2} \left(\|\beta_{i1}\|^2 + \Delta\tau_{i,\max}^2 \right)
\end{aligned} \tag{56}$$

Substituting Equation (56) into (55), we obtain:

$$\begin{aligned}
\dot{V}_i \leq & \sum_{i=1}^{n} \{ \dot{V}_{io} - \lambda_{\min}(K_{i1}) \sum_{l=1}^{3} \ln \frac{k_{ib,l}^2}{k_{ib,l}^2 - z_{i1,l}^2} \\
& - \left(\lambda_{\min}(K_{i2}) - \frac{a_{id} + \lambda_{\max}(K_{oi2})}{2} \right) \|z_{i2}\|^2 \\
& - \left(\lambda_{\min}(L_{i1}) - \frac{a_{id} + \lambda_{\max}(\overline{M}_i^{-1})}{2} \right) \|\beta_{i1}\|^2 \\
& + \frac{\lambda_{\max}(K_{oi2})}{2} \|\tilde{\eta}_i\|^2 + \frac{a_{id} + d_i}{2} \|\tilde{v}_i\|^2 \\
& + \frac{a_{id}}{2} q_{i,\max}^2 + \frac{\lambda_{\max}(\overline{M}_i^{-1})}{2} \Delta\tau_{i,\max}^2 \} \\
\leq & \sum_{i=1}^{n} \{ \dot{V}_{io} - b_{i1} \sum_{l=1}^{3} \ln \frac{k_{ib,l}^2}{k_{ib,l}^2 - z_{i1,l}^2} - b_{i2} \|z_{i2}\|^2 \\
& - b_{i3} \|\beta_{i1}\|^2 + b_{i4} \|\tilde{\eta}_i\|^2 + b_{i5} \|\tilde{v}_i\|^2 + b_{i6} \} \\
\leq & \sum_{i=1}^{n} \{ \dot{V}_{io} - b_{i1} \sum_{l=1}^{3} \ln \frac{k_{ib,l}^2}{k_{ib,l}^2 - z_{i1,l}^2} - b_{i2} \|z_{i2}\|^2 \\
& - b_{i3} \|\beta_{i1}\|^2 + \lambda_{\max}(A_{i1}) \|\chi_i\|^2 + b_{i6} \}.
\end{aligned} \tag{57}$$

where we select appropriate parameters K_{i1}, K_{i2}, K_{oi2} and L_{i1} to meet:

$$b_{i1} = \lambda_{\min}(K_{i1}) > 0, \tag{58}$$

$$b_{i2} = \lambda_{\min}(K_{i2}) - \frac{a_{id} + \lambda_{\max}(K_{oi2})}{2} > 0, \tag{59}$$

$$b_{i3} = \lambda_{\min}(L_{i1}) - \frac{a_{id} + \lambda_{\max}(\overline{M}_i^{-1})}{2} > 0, \tag{60}$$

$$b_{i4} = \frac{\lambda_{\max}(K_{oi2})}{2} > 0, \tag{61}$$

$$b_{i5} = \frac{a_{id} + d_i}{2} > 0, \tag{62}$$

and $b_{i6} = \frac{a_{id}}{2} q_{i,\max}^2 + \frac{\lambda_{\max}(\overline{M}_i^{-1})}{2} \Delta\tau_{i,\max}^2$, $A_{i1} = \mathrm{diag}\{b_{i4}, b_{i5}\}$.

Substituting Equation (40) into (57), we obtain

$$\begin{aligned}\dot{V}_i \le& \sum_{i=1}^{n}\{-a_{i1}V_{io} - b_{i1}\sum_{l=1}^{3}\ln\frac{k_{ib,l}^2}{k_{ib,l}^2 - z_{i1,l}^2} - b_{i2}\|z_{i2}\|^2 \\ &- b_{i3}\|\beta_{i1}\|^2 + \lambda_{\max}(A_{i1})\|\chi_i\|^2 + a_{i2} + b_{i6}\} \\ \le& \sum_{i=1}^{n}\{-\left(a_{i1} - \frac{\lambda_{\max}(A_{i1})}{\lambda_{\min}(P_i)}\right)V_{io} \\ &- b_{i1}\sum_{l=1}^{3}\ln\frac{k_{ib,l}^2}{k_{ib,l}^2 - z_{i1,l}^2} - b_{i2}\|z_{i2}\|^2 \\ &- b_{i3}\|\beta_{i1}\|^2 + a_{i2} + b_{i6}\} \\ \le& -c_{i1}V_i + c_{i2}\end{aligned} \tag{63}$$

As a result of the above control low, $\dot{V}_i \le -c_{i1}V_i + c_{i2}$ and this results in the ultimately uniformly bounded regulation of the state.

Then, Equation (63) can be written as

$$\dot{V}_{io}(t) \le -c_{i1}V_{io}(t) + c_{i2}, \tag{64}$$

where $c_{i1} = \min\left\{a_{i1} - \frac{\lambda_{\max}(A_{i1})}{\lambda_{\min}(P_i)}, 2b_{i1}, \frac{2b_{i2}}{\lambda_{\max}(\bar{M}_i)}, 2b_{i3}\right\} > 0$, and $c_{i2} = \sum_{i=1}^{n}\{a_{i2} + b_{i6}\}$, $0 < c_{i2} \le c_{i2,\max}$ with $c_{i2,\max} \in \mathbf{R}$ being a positive constant.

The coefficients in the controller design process are determined by Equation (64). Since the controller design process needs to meet the Lyapunov theory, the selection of parameters needs to meet Equation (64).

From the Equation (64), when $t \to \infty$, $V_{io} \to \frac{c_{i2}}{c_{i1}}$. Then, Equation (64) becomes

$$V_{io}(t) \le \left[V_{io}(0) - \frac{c_{i2}}{c_{i1}}\right]e^{-c_{i1}t} + \frac{c_{i2}}{c_{i1}}, \tag{65}$$

According to the definition of the Lyapunov function V_i and Theorem 1, it can be concluded that χ_i, $\tilde{W}_i$, z_{i2}, β_{i1} and $\ln\frac{k_{ib,l}^2}{k_{ib,l}^2 - z_{i1,l}^2}$ are bounded, where $\ln\frac{k_{ib,l}^2}{k_{ib,l}^2 - z_{i1,l}^2}$ implies that z_{i1} always remains within the set $\Omega_{z_{i1}}$. Therefore, all signals in the closed-loop system are uniformly ultimately bounded.

Therefore, conclusion (i) is valid.

We now prove (ii) of Theorem 2. The tracking error of the ith USV in the earth-fixed frame is defined as $\delta_i = \eta_i - \eta_d - \mu_i$. According to the definition of z_{i1} in Equation (45), we have

$$z_1 = (\mathcal{H} \otimes I_3)\delta, \tag{66}$$

where $z_1 = [z_{11}^{\mathrm{T}}, z_{21}^{\mathrm{T}}, \ldots, z_{n1}^{\mathrm{T}}]^{\mathrm{T}}$ and $\delta = [\delta_1^{\mathrm{T}}, \delta_2^{\mathrm{T}}, \ldots, \delta_n^{\mathrm{T}}]^{\mathrm{T}}$. $\mathcal{H}$ is defined in Section 2.1.

According to Assumption 1, all eigenvalues of matrix $\mathcal{H}$ have positive real parts. Thus, we obtain

$$\|\delta\| \le \frac{\|z_1\|}{\lambda_{\min}(\mathcal{H})} \tag{67}$$

According to Equation (63), the variable z_{i1} satisfies $\|z_{i1}\| \le \sqrt{c_{i2,\max}/b_{i1}}$. Therefore, δ is bounded. Thus, all USVs track the reference signal with a bounded tracking error. These prove that ii) holds.

From the Lemma 1 and BLF candidate $\ln\frac{k_{ib,l}^2}{k_{ib,l}^2 - z_{i1,l}^2}$, we obtain $|z_{i1,l}| < k_{ib,l}$, i.e., $-k_{ib,l} < z_{i1,l} < k_{ib,l}$.

Using Equation (66) and $\delta_i = \eta_i - \eta_d - \mu_i$, we have

$$\eta_i \leq \frac{k_{ib}}{\lambda_{\min}(\mathcal{H})} + \eta_d + \mu_i \tag{68}$$

Let $k_{ic} = \frac{k_{ib}}{\lambda_{\min}(\mathcal{H})} + \eta_d + \mu_i$. That is, the output of each USV is always kept in set $\Omega_{\eta_i} = \{\eta_i \mid -k_{ic} < \eta_i < k_{ic}\}$. Therefore, conclusion iii) is valid.

This completes the proof. □

5. Simulation Results

Simulations are carried out with Matlab 2018a. The simulations are run on a PC with a dual-core 2.30 GHz Intel(R) Core(TM) i5-8300H CPU and 8 GB of RAM.

In this section, we simulate a USV swarm consisting of one virtual leader vehicle (indexed by 0) and four follower USVs (indexed by $1, 2, 3, 4, 5, 6$) to demonstrate the effectiveness of the proposed method. The directed communication graph is shown in Figure 3.

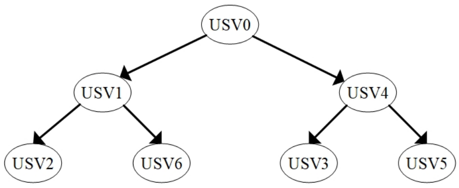

Figure 3. Directed communication topology.

In simulations, the model of surface ship Cybership II is used [42]. The time-varying environmental disturbances are modeled as a first-order Markov process [40]. The control forces and moment are limited as $\tau_{i1,\max} = -\tau_{i1,\min} = 2$ N, $\tau_{i2,\max} = -\tau_{i2,\min} = 2$ N and $\tau_{i3,\max} = -\tau_{i3,\min} = 1.5$ Nm. The constraint k_{ib} is set as $k_{ib} = [0.6\text{ m}, 0.6\text{ m}, 0.2\text{ rad}]^{\mathrm{T}}$. The desired reference trajectory η_d is generated as Equation (69). Some parameters are set as shown in Table 2.

$$\eta_d = \begin{cases} [\frac{t}{10}, 0, 0], 0 \leq t < 50; \\ [5\ \sin(\frac{1}{50}(t-50)) + 5, -5\ \cos(\frac{1}{50}(t-50)) + 5, \frac{1}{50}(t-50)], \\ 50 \leq t < 50 + 50\pi; \\ [-5\ \sin(\frac{1}{50}(t-50-50\pi)) + 5, -5\ \cos(\frac{1}{50}(t-50-50\pi)) + 15, \\ \frac{1}{50}(t-50-50\pi)], 50 + 50\pi \leq t < 50 + 100\pi; \\ [\frac{1}{10}(t-50-100\pi), 20, 0], 50 + 100\pi \leq t \leq 400; \end{cases} \tag{69}$$

Table 2. The parameters of six USVs.

μ_i	Parameters/(m, m, rad)	η_i	Parameters/(m, m, rad)
μ_1	$[1.2, 0, 0]^{\mathrm{T}}$	η_1	$[1.4, 0.2, \pi/5]^{\mathrm{T}}$
μ_2	$[0.6, 1.2, 0]^{\mathrm{T}}$	η_2	$[0.7, 1.0, \pi/5]^{\mathrm{T}}$
μ_3	$[-0.6, 1.2, 0]^{\mathrm{T}}$	η_3	$[-0.7, 1.0, \pi/5]^{\mathrm{T}}$
μ_4	$[-1.2, 0, 0]^{\mathrm{T}}$	η_4	$[-1.3, 0.2, \pi/5]^{\mathrm{T}}$
μ_5	$[-0.6, -1.2, 0]^{\mathrm{T}}$	η_5	$[-0.5, -1.5, \pi/5]^{\mathrm{T}}$
μ_6	$[0.6, -1.2, 0]^{\mathrm{T}}$	η_6	$[0.7, -1.5, \pi/5]^{\mathrm{T}}$

5.1. Performance of Proposed Control Strategy

In this subsection, the simulation results are given to verify the performance of the proposed control strategy. The parameters of environmental disturbance are selected as T =

$diag\{10^{-3}, 10^{-3}, 10^{-3}\}$, $b(0) = [0, 0, 0]^{\mathrm{T}}$, $\mathrm{E}_b = diag\{10^{-5}, 10^{-5}, 10^{-5}\}$, $\vartheta_b = [0.1, 0.1, 0.1]^{\mathrm{T}}$. The parameters of the observer are selected as $K_{oi1} = diag\{30, 30, 30\}$, $K_{oi2} = diag\{30, 30, 30\}$, $\gamma_i = 1000$ and $k_i = 0.2$. The parameters of the controller are chosen as $\iota_i = 0.001$, $K_{i1} = diag\{0.6, 0.6, 0.6\}$ and $K_{i2} = diag\{1.1, 1.1, 1.1\}$.

The simulation results are shown in Figures 4–8. Figure 4 shows the trajectories of six USVs under time-varying environmental disturbance and input saturation. It can be shown that, after adjustment, the position and heading of six USVs can reach the present point, maintain the desired relative position between each other, and realize the swarm control of multiple USVs in a fixed formation, even if there is a position and heading deviation at the initial time. Figure 5 describes the tracking errors of four USVs, including the position and heading. It can be seen from Figure 5 that the tracking error is convergent. Figure 6 shows the control input of six USVs. According to the analysis of Figure 6, the control input is limited within the range of input constraints. Therefore, the input saturation can be realized using the ADS designed in this paper.

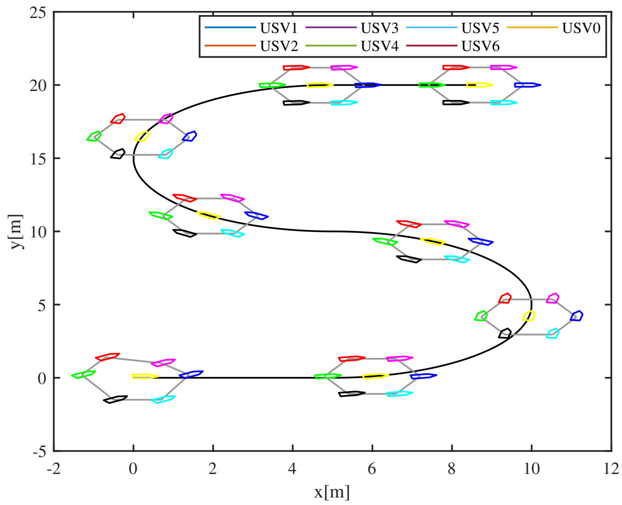

Figure 4. Trajectories of six USVs.

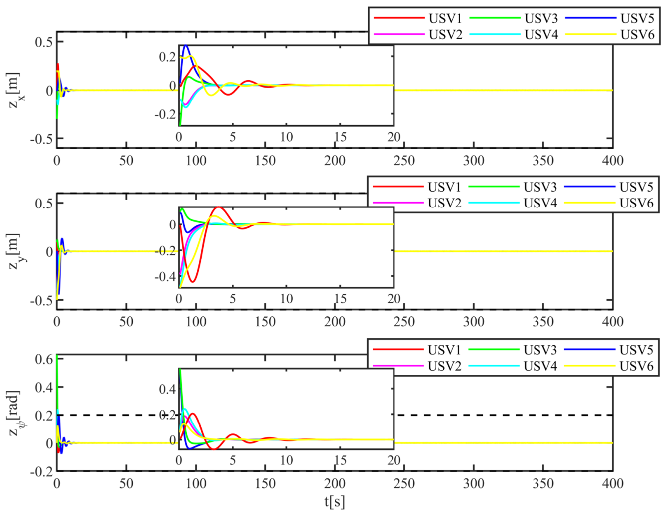

Figure 5. Tracking errors of six USVs.

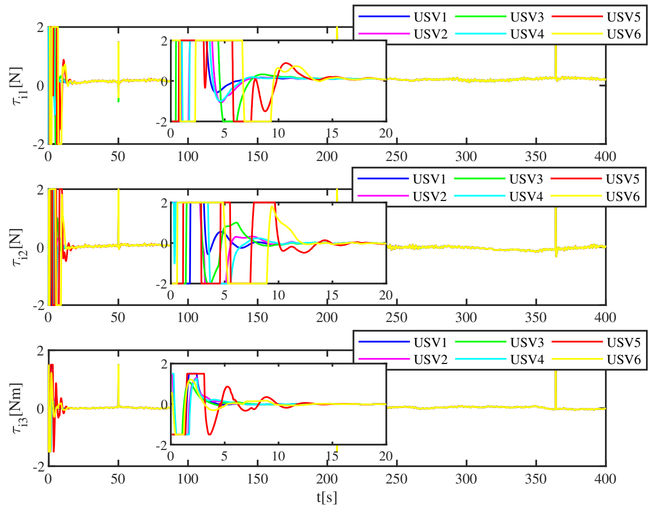

Figure 6. Control input of six USVs.

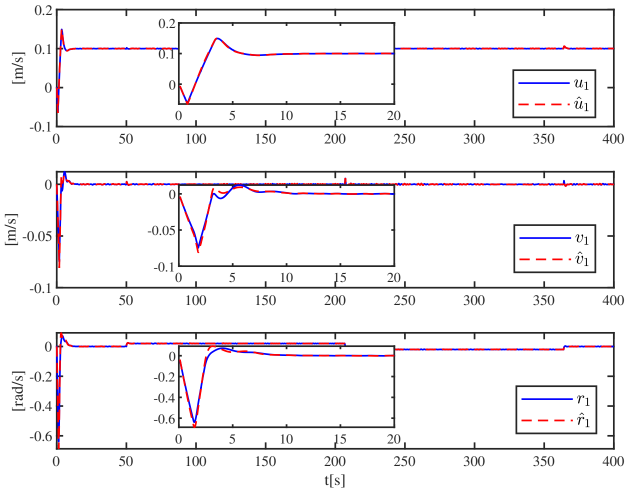

Figure 7. Velocity estimation performance of NASO with solid lines for the real states and dashed lines for their estimation.

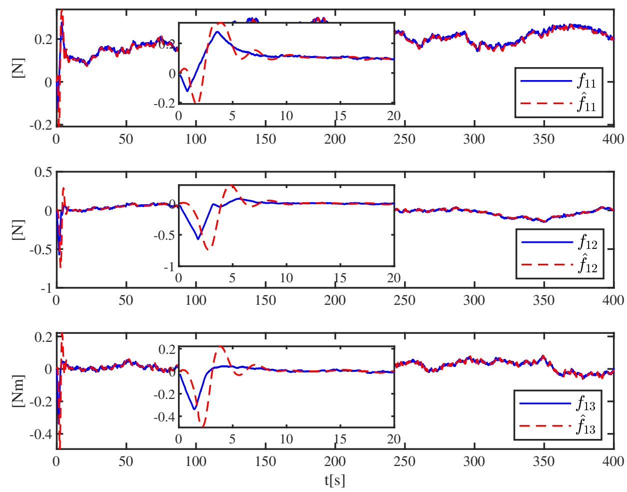

Figure 8. Total unknown function estimation performance of NASO with solid lines for the real states and dashed lines for their estimation.

Taking USV 1 as an example, the estimation effects of the observer are shown in Figures 7 and 8. Figure 7 depicts the comparison effect between the real value and the estimated value of the velocity. The solid lines and dashed line represent the real value and estimated value, respectively. It can be seen from Figure 7 that the designed NASO is effective and can realize the estimation of speed. Figure 8 describes the real values and estimated values of the total unknown function acting on the first USV. It can be seen from Figure 8 that the NASO is stable despite boundary estimate errors.

5.2. Comparison Group

To further illustrate the effectiveness of the proposed control strategy, a neural adaptive dynamic surface control (NADSC) approach without ADS is considered, whose motion is described by

$$\begin{cases} z_{i1} = \sum\limits_{j \in \mathcal{N}_i} a_{ij}(\eta_i - \eta_j - \mu_{ij}) + a_{i0}(\eta_i - \eta_d - \mu_i) \\ \alpha_i = \dfrac{R_i^{\mathrm{T}}}{a_{id}} \left\{ -K_{i1} z_{i1} - \kappa_{ia} z_{i3} + \sum\limits_{j \in \mathcal{N}_i} a_{ij} R_j \hat{v}_j + a_{i0} \dot{\eta}_d \right\} \\ \dot{v}_{ir} = v_{ir}^d = -\iota_i^2 (v_{ir} - \alpha_i) \\ z_{i2} = \hat{v}_i - v_{ir} \\ \tau_{ic} = -K_{i2} z_{i2} + \hat{W}_i h_{ij}(\varsigma_i) + \overline{M}_i v_{ir}^d \end{cases} \tag{70}$$

where the parameters are set to be the same as the proposed controller.

The simulation results are shown in Figures 9–11. Figure 9 describes the tracking error of six USVs without ADS. Compared with Figure 5, it can be concluded that the tracking error fluctuates greatly at 0–10 s. Figure 10 shows the control input of six USVs without ADS. Compared with Figure 6, it can be concluded that the control input fluctuates greatly at 0–10 s. Figure 11 depicts the control inputs of six USVs without input constraints. It can be seen from Figure 11 that the maximum control force and moment is $\tau_i = [\tau_{i1}, \tau_{i2}, \tau_{i3}]^{\mathrm{T}} = [200\ \mathrm{N}, 200\ \mathrm{N}, 150\ \mathrm{Nm}]^{\mathrm{T}}$. Compared with Figure 6, the maximum control force and torque of the USV were exceeded.

To summarize, the proposed approach combining the NASO, ADS and LBF successfully handled the output feedback swarm control problem with satisfactory results.

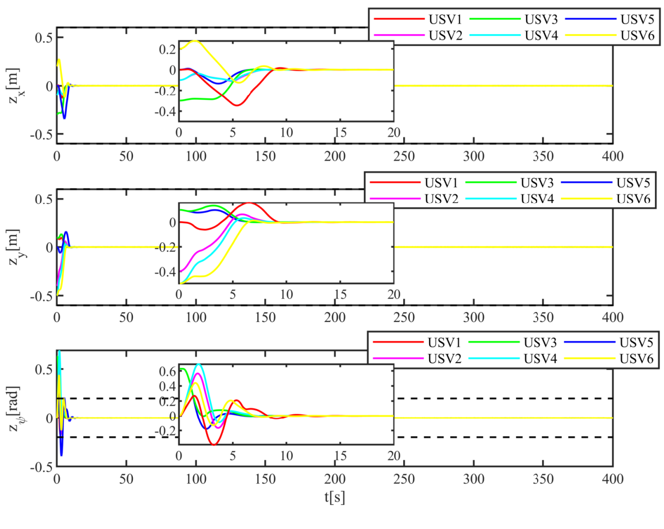

Figure 9. Tracking errors of six USVs using NADSC without ADS.

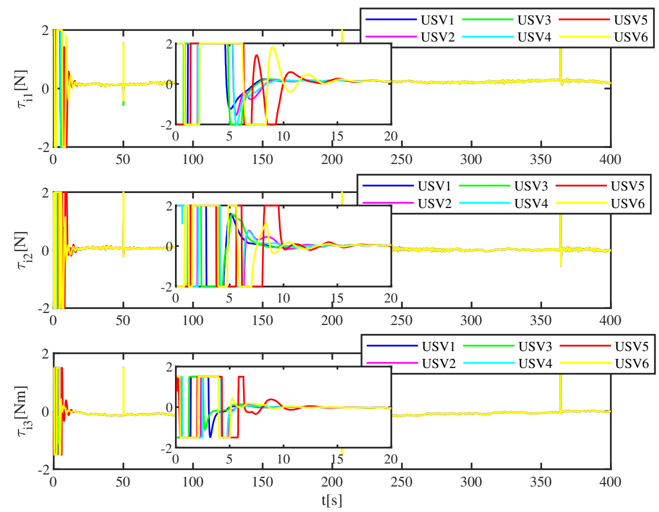

Figure 10. Control input of six USVs using NADSC without ADS.

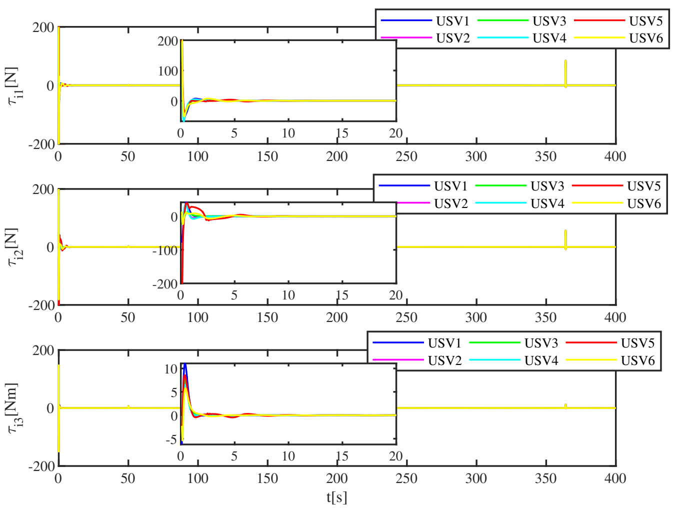

Figure 11. Control input of six USVs using NADSC without ADS and input constraint.

6. Conclusions

This paper investigated swarm control for USVs in the presence of model uncertainty, the unavailability of velocity measurements, unknown environmental disturbances, input saturation and output constraints. NASO is designed to estimate the unknown model uncertainty, unmeasured velocity and unknown environmental disturbance. ADS is introduced to mitigate the input saturation problem. An output feedback controller is designed, which is composed of NASO, ADS, SOLTD and BLF. The stability of the system is proved via the Lyapunov method. Finally, the effectiveness of the proposed control strategy is verified in simulation. However, in the process of designing the output feedback controller, we do not take the problem of obstacle avoidance into account. Then, this will be the focus of our research.

Author Contributions: Conceptualization, G.X. and X.S.; methodology, X.S.; software, X.S. and X.X.; formal analysis, X.S. and X.X.; investigation, X.S.; supervision, G.X. and X.X.; funding acquisition, G.X. All authors have read and agreed to the published version of the manuscript.

Funding: This work was supported by the 7th Generation Ultra Deep Water Drilling Unit Innovation Project.

Institutional Review Board Statement: Not applicable.

Informed Consent Statement: Not applicable.

Data Availability Statement: Data are contained within the article.

Conflicts of Interest: The authors declare no conflict of interest.

Abbreviations

The following abbreviations are used in this manuscript:

USV	unmanned surface vehicle
BLF	barrier Lyapunov function
NN	neural network
NASO	neural adaptive state observer
LMIs	linear matrix inequalities
SOLTD	second-order linear tracking differentiator
ADS	auxiliary dynamic system
NADSC	neural adaptive dynamic surface control

References

1. Peng, Z.; Wang, J.; Wang, D. Distributed containment maneuvering of multiple marine vessels via neurodynamics-based output feedback. *IEEE Trans. Ind. Electron.* **2017**, *64*, 3831–3839. [CrossRef]
2. Mahacek, P.; Kitts, C.A.; Mas, I. Dynamic Guarding of Marine Assets Through Cluster Control of Automated Surface Vessel Fleets. *IEEE/ASME Trans. Mechatron.* **2012**, *17*, 65–75. [CrossRef]
3. Raboin, E.; Švec, P.; Nau, D.S.; Gupta, S.K. Model-predictive asset guarding by team of autonomous surface vehicles in environment with civilian boats. *Auton. Robot.* **2014**, *38*, 261–282. [CrossRef]
4. Kim, Y.H; Lee, S.W.; Yang, H.S.; Shell, D.A. Toward autonomous robotic containment booms: Visual servoing for robust inter-vehicle docking of surface vehicles. *Intell. Serv. Robot.* **2012**, *5*, 1–18. [CrossRef]
5. Zoss, B.M.; Mateo, D.; Kuan, Y.K.; Tokić, G.; Ghamanbaz, M.; Goh, L.; Vallegra, F.; Bouffanais, R.; Yue, D.K.P. Distributed system of autonomous buoys for scalable deployment and monitoring of large waterbodies. *Auton. Robot.* **2018**, *42*, 1669–1689. [CrossRef]
6. Chamanbaz, M.; Notarstefano, G.; Bouffanais, R. A randomized distributed ellipsoid algorithm for uncertain feasibility problems. In Proceedings of the 2017 IEEE 56th Annual Conference on Decision and Control, Melbourne, Australia, 12–15 December 2017; pp. 1305–1310.
7. Zhang, L.J.; Jia, H.-M.; Qi, X. NNFFC-adaptive output feedback trajectory tracking control for a surface ship at high speed. *Ocean. Eng.* **2011**, *38*, 1430–1438. [CrossRef]
8. Li, J.; Ren, W.; Xu, S. Distributed containment control with multiple dynamic leaders for double-integrator dynamics using only position measurements. *IEEE Trans. Autom. Control* **2012**, *57*, 1553–1559. [CrossRef]
9. Ihle, I.A.F.; Skjetne, R.; Fossen, T.I. Output feedback control for maneuvering systems using observer backstepping. In Proceedings of the 13th Mediterranean Conference on Control and Automation, Limassol, Cyprus, 27–28 June 2005; pp. 1512–1517.
10. Dai, S.L.; Wang, M.; Wang, C.; Li, L. Learning from adaptive neural network output feedback control of uncertain ocean surface ship dynamics. *Int. J. Adapt. Control. Signal Process.* **2014**, *28*, 341–365. [CrossRef]
11. Wei, H.; Zhao, Y.; Sun, C. Adaptive Neural Network Control of a Marine Vessel With Constraints Using the Asymmetric Barrier Lyapunov Function. *IEEE Trans. Cybern.* **2017**, *47*, 1641–1651.
12. Du, J.; Hu, X.; Liu, H.; Chen, C. L. Adaptive Robust Output Feedback Control for a Marine Dynamic Positioning System Based on a High-Gain Observer. *IEEE Trans. Neural Netw. Learn. Syst.* **2015**, *26*, 2775–2786. [CrossRef]
13. Xia, G.; Shao, X.; Zhao, A. Robust Nonlinear Observer Furthermore, Observer-Backstepping Control Design For Surface Ships. *Asian J. Control.* **2015**, *17*, 1377–1393. [CrossRef]
14. Zhang, J.; Yu, S.; Yan, Y. Fixed-time output feedback trajectory tracking control of marine surface vessels subject to unknown external disturbances and uncertainties. *ISA Trans.* **2019**, *93*, 145–155. [CrossRef]
15. Li, X.; Shi, P.; Wang, Y. Distributed cooperative adaptive tracking control for heterogeneous systems with hybrid nonlinear dynamics. *Nonlinear Dyn.* **2018**, *95*, 2131–2141. [CrossRef]
16. Xia, G.; Sun, C.; Zhao, B.; Xia, X.; Sun, X. Neuroadaptive Distributed Output Feedback Tracking Control for Multiple Marine Surface Vessels With Input and Output Constraints. *IEEE Access* **2019**, *7*, 123076–123085. [CrossRef]
17. Peng, Z.; Wang, D.; Liu, H.H.T.; Sun, G.; Wang, H. Distributed robust state and output feedback controller designs for rendezvous of networked autonomous surface vehicles using neural networks. *Neurocomputing* **2013**, *115*, 130–141. [CrossRef]
18. Lin, X.; Wang, Y.; Liu, Y. Neural-network-based robust terminal sliding-mode control of quadrotor. *Asian J. Control* **2022**, *24*, 427–438. [CrossRef]
19. Yan, Z.; Wang, M.; Xu, J. Global adaptive neural network control of underactuated autonomous underwater vehilces with parametric modeling uncertainty. *Asian J. Control* **2019**, *21*, 1342–1354. [CrossRef]

20. Seshagiri, S.; Khalil, H.K. Output feedback control of nonlinear systems using RBF neural networks. *IEEE Trans. Neural Netw.* **2000**, *11*, 69–79. [CrossRef]
21. Lu, Y.; Zhang, G.; Sun, Z.; Zhang, W. Adaptive cooperative formation control of autonomous surface vessels with uncertain dynamics and external disturbances. *Ocean Eng.* **2018**, *167*, 36–44. [CrossRef]
22. Tee, K.P.; Ge, S.S. Control of fully actuated ocean surface vessels using a class of feedforward approximators. *IEEE Trans. Control. Syst. Technol.* **2006**, *14*, 750–756. [CrossRef]
23. Kahveci, N.E.; Ioannou, P. A. Adaptive steering control for uncertain ship dynamics and stability analysis. *Automatica* **2013**, *49*, 685–697. [CrossRef]
24. Chen, M.; Tao, G.; Jiang B. Dynamic Surface Control Using Neural Networks for a Class of Uncertain Nonlinear Systems With Input Saturation. *IEEE Trans. Neural Netw. Learn. Syst.* **2015**, *29*, 2086–2097. [CrossRef] [PubMed]
25. Huang, B.; Song, S.; Zhu, C.; Li, J.; Zhou, B. Finite-time distributed formation control for multiple unmanned surface vehicles with input saturation. *Ocean Eng.* **2021**, *233*, 109158. [CrossRef]
26. Zhou, W.; Wang, Y.; Ahn, C.K.; Cheng, J.; Chen, C. Adaptive Fuzzy Backstepping-Based Formation Control of Unmanned Surface Vehicles With Unknown Model Nonlinearity and Actuator Saturation. *IEEE Trans. Veh. Technol.* **2020**, *69*, 14749–14764. [CrossRef]
27. Xia, G.; Xia, X.; Zhao, B.; Sun, C.; Sun, X. Distributed Tracking Control for Connectivity-Preserving and Collision-Avoiding Formation Tracking of Underactuated Surface Vessels with Input Saturation. *Appl. Sci.* **2020**, *10*, 3372. [CrossRef]
28. Do, K.D. Formation Tracking Control of Unicycle-Type Mobile Robots With Limited Sensing Ranges. *IEEE Trans. Control. Syst. Technol.* **2008**, *16*, 527–538. [CrossRef]
29. Do, K.D. Practical formation control of multiple underactuated ships with limited sensing ranges. *Robot. Auton. Syst.* **2011**, *59*, 457–471. [CrossRef]
30. Hu, H.; Yoon, S.Y.; Lin, Z. Coordinated Control of Wheeled Vehicles in the Presence of a Large Communication Delay Through a Potential Functional Approach. *IEEE Trans. Intell. Transp. Syst.* **2014**, *15*, 2261–2272. [CrossRef]
31. Yoo, S.J.; Kim, T.-H. Distributed formation tracking of networked mobile robots under unknown slippage effects. *Automatica* **2015**, *54*, 100–106. [CrossRef]
32. Huang, Y.; Ding, H.; Zhang, Y.; Wang, H.; Cao, D.; Xu, N.; Hu, C. A Motion Planning and Tracking Framework for Autonomous Vehicles Based on Artificial Potential Field Elaborated Resistance Network Approach. *IEEE Trans. Ind. Electron.* **2020**, *67*, 1376–1386. [CrossRef]
33. Tee, K.P.; Ge, S.S. Control of nonlinear systems with partial state constraints using a barrier Lyapunov function. *Int. J. Control* **2011**, *84*, 2008–2023. [CrossRef]
34. Ghommam, J.; Saad, M. Adaptive Leader–Follower Formation Control of Underactuated Surface Vessels Under Asymmetric Range and Bearing Constraints. *IEEE Trans. Veh. Technol.* **2018**, *67*, 852–865. [CrossRef]
35. Park, B.S.; Yoo, S.J. An Error Transformation Approach for Connectivity-Preserving and Collision-Avoiding Formation Tracking of Networked Uncertain Underactuated Surface Vessels. *IEEE Trans. Cybern.* **2019**, *49*, 2955–2966. [CrossRef]
36. Yu, J.; Zhao, L.; Yu, H.; Lin, C. Barrier Lyapunov functions-based command filtered output feedback control for full-state constrained nonlinear systems. *Automatica* **2019**, *105*, 71–79. [CrossRef]
37. Zhang, X.; Liu, L.; Feng, G. Leader–follower consensus of time-varying nonlinear multi-agent systems. *Automatica* **2015**, *52*, 8–14. [CrossRef]
38. Liu, Y.; Lu, S.; Tong, S.; Chen, X.; Chen, C.L.P.; Li, D. Adaptive control-based Barrier Lyapunov Functions for a class of stochastic nonlinear systems with full state constraints. *Automatica* **2018**, *87*, 83–93. [CrossRef]
39. Fossen, T.I.; Strand, J.P. Passive nonlinear observer design for ships using Lyapunov methods: Full-Scale experiments with a supply vessel. *Automatica* **1999**, *35*, 3–16. [CrossRef]
40. Fossen, T.I. How to incorporate wind, waves and ocean currents in the marine craft equations of motion. In Proceedings of the 9th IFAC Conference on Manoeuvring and Control of Marine Craft, Arenzano, Italy, 19–21 September 2012; pp. 126–131.
41. Park, B.S.; Yoo, S.J.; Park, J.B.; Choi, Y.H. Adaptive neural sliding mode control of nonholonomic wheeled mobile robots with model uncertainty. *IEEE Trans. Control. Syst. Technol.* **2009**, *17*, 207–214. [CrossRef]
42. Skjetne, R.; Kokotović, P.V. Adaptive maneuvering, with experiments, for a model ship in a marine control laboratory. *Automatica* **2005**, *41*, 289–298. [CrossRef]